© 2017. Published by The Company of Biologists Ltd | Journal of Experimental Biology (2017) 220, 4213-4224 doi:10.1242/jeb.167700

RESEARCH ARTICLE

It's not all black and white: visual scene parameters influence optokinetic reflex performance in *Xenopus laevis* tadpoles

Céline M. Gravot[1,2,*,‡], Alexander G. Knorr[3,4,*], Stefan Glasauer[3] and Hans Straka[1]

ABSTRACT

The maintenance of visual acuity during active and passive body motion is ensured by gaze-stabilizing reflexes that aim at minimizing retinal image slip. For the optokinetic reflex (OKR), large-field visual motion of the surround forms the essential stimulus that activates eye movements. Properties of the moving visual world influence cognitive motion perception and the estimation of visual image velocity. Therefore, the performance of brainstem-mediated visuo-motor behaviors might also depend on image scene characteristics. Employing semi-intact preparations of mid-larval stages of *Xenopus laevis* tadpoles, we studied the influence of contrast polarity, intensity, contour shape and different motion stimulus patterns on the performance of the OKR and multi-unit optic nerve discharge during motion of a large-field visual scene. At high contrast intensities, the OKR amplitude was significantly larger for visual scenes with a positive contrast (bright dots on a dark background) compared with those with a negative contrast. This effect persisted for luminance-matched pairs of stimuli, and was independent of contour shape. The relative biases of OKR performance along with the independence of the responses from contour shape were closely matched by the optic nerve discharge evoked by the same visual stimuli. However, the multi-unit activity of retinal ganglion cells in response to a small single moving vertical edge was strongly influenced by the light intensity in the vertical neighborhood. This suggests that the underlying mechanism of OKR biases related to contrast polarity directly derives from visual motion-processing properties of the retinal circuitry.

KEY WORDS: Motion perception, Vision, Image features, Contrast polarity

INTRODUCTION

Most vertebrates live and locomote within highly dynamic and structured environments composed of animate and inanimate objects. To ensure constant visual acuity during locomotion and passive perturbations of the head and/or body, retinal images are stabilized by brainstem-mediated ocular motor reflexes. The vestibulo-ocular reflex (VOR) operates best at high frequencies and accelerations and elicits compensatory eye movements following stimulation of the vestibular sensory system (Straka and Dieringer, 2004). This open-loop reflex is supplemented by a visuo-motor reflex, the optokinetic reflex (OKR), which is activated by large-field visual motion and aims at minimizing the residual retinal image drift (Collewijn, 1969; Dieringer and Precht, 1982). Accordingly, the OKR plays an important role in gaze stabilization, in particular at low frequencies and/or velocities of visual image motion. The OKR in all vertebrates is subject to two requirements: providing a rapid processing of image motion while maintaining a faithful representation of the actual image velocity over a broad range of viewing conditions. Visual stimuli can range from, for example, bright sunlight to dusk/dawn or from clear to murky water in aquatic environments. These conditions have vastly different visual scene characteristics such as contrast intensity and polarity as well as total luminance. Some of these features are already known to influence visual motion-driven reflexes and perception capabilities (Donaghy, 1980). Contrarily, the influence of contrast polarity, i.e. the sign of brightness differences between objects and background, or contrast intensity on the performance of the OKR is only poorly understood.

The influence of the various visual scene properties on OKR performance might be due to a differential processing within the underlying brainstem network or derive already from the retinal motion detection system. As support for the latter, manipulation of visual scene characteristics can lead to a differential excitation of retinal photoreceptors, which in turn might elicit specific activation patterns in motion-sensitive retinal ganglion cells (Enroth-Cugell and Robson, 1966) and thus generate a different velocity estimate. Furthermore, the center-surround organizational feature of retinal edge detectors allows the assumption that the properties of a uniform background in the visual objects' neighborhood influence the extraction of motion information from small moving edges. In fact, within visual image textures, only the edges of moving particles generate a motion percept, while the large uniform areas of the large-field image (which can be construed as background) make no immediate contribution to visual motion perception (Adelson and Bergen, 1985). These scene-related differences in retinal speed estimation might then translate into differences in signal processing within brainstem circuits and thus into behavioral responses, such as the OKR.

Here, we studied the influence of image scene properties on OKR performance in tadpoles of the African clawed toad *Xenopus laevis* Daudin 1802. These vertebrates allow the study of visuo-motor transformations in semi-intact preparations that offer a facilitated accessibility to all synaptic levels of the neuronal network (Straka and Simmers, 2012; von Uckermann et al., 2016). Presentation of visual scenes, randomly scattered with particles of filled closed contours (e.g. dots, squares or crescent shapes), elicited eye movements with amplitudes that depended on contrast polarity and intensity as well as luminance levels. Recordings of multi-unit spike discharge from the optic nerve of isolated eyes revealed similar dependencies from the tested stimulus parameters, suggesting that major differences in OKR performance derive from the signal processing within retinal circuits.

[1]Department Biology II, Ludwig-Maximilians-Universität München, Großhaderner Str. 2, 82152 Planegg, Germany. [2]Graduate School of Systemic Neurosciences, Ludwig-Maximilians-Universität München, Großhaderner Str. 2, 82152 Planegg, Germany. [3]Center for Sensorimotor Research, Department of Neurology, University Hospital Munich, Feodor-Lynen-Str. 19, 81377 Munich, Germany. [4]Institute for Cognitive Systems, TUM Department of Electrical and Computer Engineering, Technical University of Munich, Karlstr. 45/II, 80333 Munich, Germany.
*These authors contributed equally to this work

‡Author for correspondence (gravot@bio.lmu.de)

C.M.G., 0000-0003-4074-850X; H.S., 0000-0003-2874-0441

Received 3 August 2017; Accepted 16 September 2017

Journal of Experimental Biology (2017) 220, 4213-4224 doi:10.1242/jeb.167700

MATERIALS AND METHODS

Animals

Experiments were performed *in vitro* on isolated, semi-intact preparations of *X. laevis* tadpoles of either sex (n=42) and complied with the National Institutes of Health publication entitled 'Principles of animal care', no. 86-23, revised 1985. Permission for these experiments was granted by the governmental institution at the Regierung von Oberbayern/Government of Upper Bavaria (permit no. 55.2-1-54-2532.3-59-12). Animals at developmental stages 52–55 (Nieuwkoop and Faber, 1994) were obtained from the in-house animal breeding facility at the Biocenter-Martinsried of the Ludwig-Maximilians-Universität München. For all experiments, tadpoles were anesthetized in 0.05% MS-222 (Pharmaq Ltd, Fordingbridge, Hampshire, UK) in frog Ringer solution (75 mmol l^{-1} NaCl, 25 mmol l^{-1} $NaHCO_3$, 2 mmol l^{-1} $CaCl_2$, 2 mmol l^{-1} KCl, 0.5 mmol l^{-1} $MgCl_2$, and 11 mmol l^{-1} glucose, pH 7.4) and decapitated at the level of the upper spinal cord.

Experimental approach

For behavioral experiments, the skin covering the dorsal head was removed, the soft skull tissue opened and the forebrain disconnected (Lambert et al., 2012). This surgical procedure anatomically preserved the remaining central nervous system and the eyes including the optic nerve, extraocular motor innervation and eye muscles. Such preparations allowed prolonged recordings of eye motion and neuronal activity and *in vivo*-like activation of the OKR by horizontal large-field image motion under controlled *in vitro* conditions. For electrophysiological recordings of retinal ganglion cell axons in these preparations, the optic nerve of the right eye was cleaned from surrounding connective tissue and transected at the level of the optic chiasm. All extraocular muscles of this eye were transected at their proximal insertion to immobilize the eye in its natural position within the head. Semi-intact preparations were allowed to recover from the surgical intervention at 14°C for 3 h (Ramlochansingh et al., 2014).

Setup

Semi-intact preparations were fixed with insect pins to the Sylgard floor of a Petri dish (5 cm diameter). The chamber, which was constantly superfused with oxygenated frog Ringer solution at a rate of 3.0–5.0 ml min^{-1}, was mechanically secured in the center of an open cylindrical screen with a height of 5 cm and a diameter of 8 cm, encompassing 275 deg of the visual field (left and right schemes in Fig. 1A). Three digital light processing (DLP) video projectors (Aiptek V60, Aiptek International GmbH, Willich, Germany), installed at 90 deg angles to each other, projected visual motion stimuli onto the screen (Packer et al., 2001) at a refresh rate of 60 Hz. For behavioral recordings, a CCD camera (Grasshopper 0.3 MP Mono FireWire 1394b, PointGrey, Vancouver, BC, Canada), mounted 20 cm above the center of the recording chamber, permitted online tracking of horizontal eye movements by custom-written software (Beck et al., 2004). The position of both eyes was digitized at a sampling rate of 50 Hz and recorded along with the visual motion stimulus (Spike2 version 7.04, Cambridge Electronic Design Ltd, Cambridge, UK). The chamber was illuminated from above using an 840 nm infrared light source. An infrared long-pass filter in the camera ensured selective transmission of infrared light and a high contrast of the eyes for motion tracking and online analysis of induced eye movements.

Electrophysiological recordings of multi-unit optic nerve spike activity were performed under the same experimental conditions. The spike discharge was recorded extracellularly (EXT 10-2F, npi Electronics, Tamm, Germany) with glass microelectrodes that were filled with Ringer solution. Electrodes were produced with a horizontal puller (P-87 Brown/Flaming, Sutter Instruments Company, Novato, CA, USA) and the tips were broken and individually adjusted to fit the respective optic nerve diameter. The multi-unit spike discharge was digitized at a sampling rate of 28.6 kHz (CED Micro1401-3, Cambridge Electronic Design Ltd) along with the visual motion stimulus. The discharge was recorded by a data acquisition program (Spike2 version 7.04, Cambridge Electronic Design Ltd).

Data processing

To assess the performance of the horizontal OKR during sinusoidal large-field visual motion stimulation, the position of both eyes was preprocessed by a Gaussian low-pass filter at a frequency of 5 Hz, and segmented into individual cycles of the stimulus, excluding all cycles with a peak eye velocity >50 deg s^{-1}. Thereby, cycles with oculomotor behaviors other than optokinetic slow phase responses, such as high-frequency horizontal oscillations during spontaneous episodes of locomotor activity (Lambert et al., 2012), were discarded. Also, four out of 42 preparations with very small OKR amplitudes (<0.5 deg s^{-1}) during the initial screening at the beginning of a recording session, likely owing to prior surgical complications, were excluded. The remaining 38 tadpoles were used for subsequent experiments. For horizontal optokinetic stimuli with sinusoidal velocity patterns, the response amplitude was computed by fitting a sinusoid of the same frequency as the stimulus to the recorded eye position trace and evaluating the amplitude of the fit. For stimulation at constant speed, the velocity of the slow-phase following eye movement was computed in a window of ±5 deg around the resting position of the eye by evaluating the slope of a least-squares fit of a straight line to the eye position trace. Additionally, the number of fast phases over the duration of the applied constant velocity visual motion stimulus (i.e. 120 s) was counted.

The rate of spontaneous and motion-evoked multi-unit spike discharge was extracted from optic nerve recordings using a threshold method. The resulting spike train was then convolved with a raised cosine window (full width at half maximum=0.5 s) to compute the firing rate. The modulation depth during sinusoidal visual motion stimulation was then computed by averaging the firing rate (F) over all cycles of a single trial, approximating the resulting average curve by a function:

$$F = a + b \times \left|\sin\left(\frac{t}{T}\right)\right|, \quad (1)$$

in which b is the modulation depth, a is the baseline firing rate and T is the period. For constant velocity visual motion stimuli, the modulation depth was computed as the difference between the maximum and the baseline firing rate.

Stimulus paradigm

Horizontal eye movements were elicited by large-field visual motion stimuli (Fig. 1A) using one of two stimulus velocity profiles. Sinusoidal visual motion stimuli with a peak velocity of ±10 deg s^{-1} and a frequency of 0.125 Hz triggered sinusoidally modulated slow conjugate following movements of both eyes (Fig. 1B). Constant velocity visual motion stimuli (120 s in temporo-nasal and naso-temporal direction, respectively) with a velocity of 10 deg s^{-1} provoked a nystagmic OKR with slow following eye movements (* in Fig. 1C) and intermittent resetting fast phases in the opposite direction (> in Fig. 1C).

Large-field horizontal visual motion stimuli consisted of grayscale random-dot (2.5 mm diameter, visual angle 1.8 deg) patterns with different tones of gray for the dots and background and

Journal of Experimental Biology

Journal of Experimental Biology (2017) 220, 4213-4224 doi:10.1242/jeb.167700

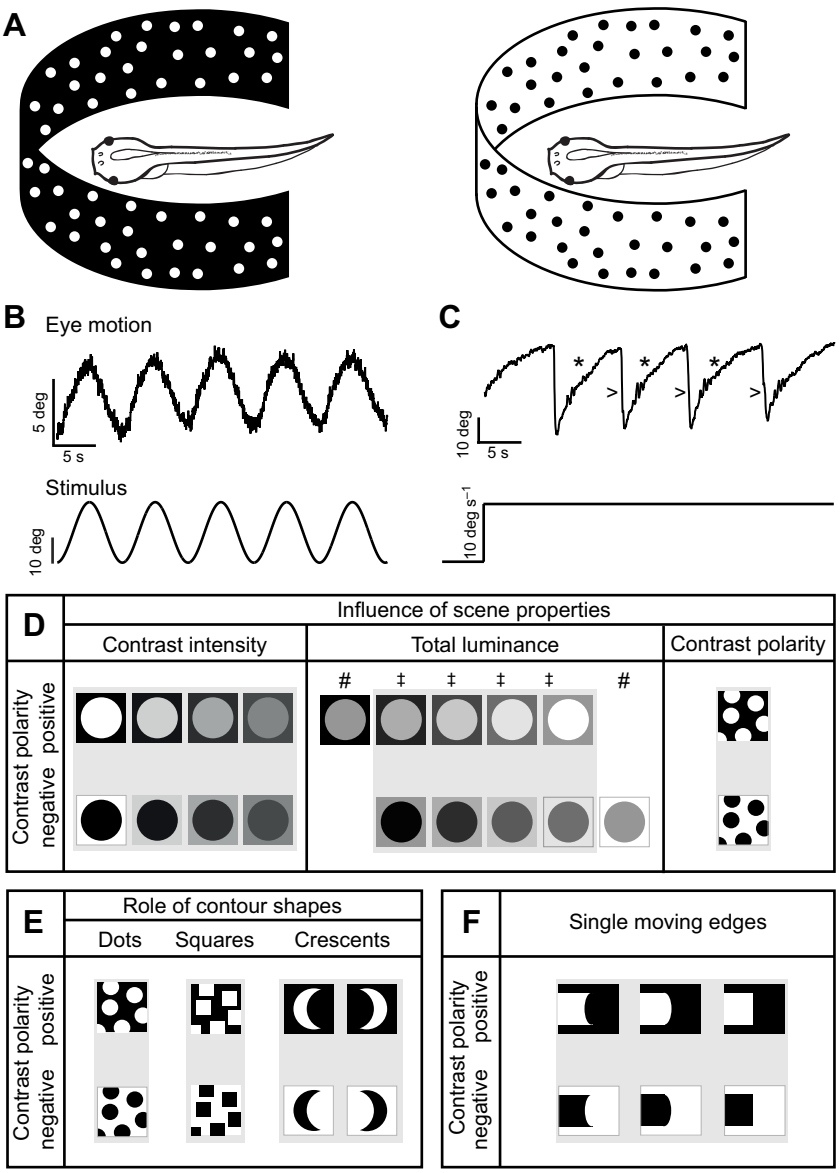

Fig. 1. Stimulation and recording paradigms of the horizontal optokinetic reflex (OKR) in *Xenopus laevis* tadpoles. (A) Schematic illustrating the experimental setting with a central recording chamber for semi-intact larval *X. laevis* preparations (adapted from Hänzi and Straka, 2016), surrounded by a cylindrical screen onto which a rotating large-field random-dot pattern with positive (white dots on black background, left) or negative (black dots on white background, right) contrast polarity is projected. (B,C) Representative examples of movements of the left eye (upper traces) evoked by sinusoidal (frequency: 0.125 Hz, peak velocity: ±10 deg s^{-1}; B) or temporo-nasal constant velocity (10 deg s^{-1}; C) visual motion stimuli (lower traces). Evoked nystagmic eye movements in C consist of slow following phases (*) interrupted by resetting fast phases (>). (D–F) Graphical illustration of variations in visual scene properties such as contrast intensity, total luminance, contrast polarity (left, middle and right panel in D, respectively), contour shapes (E) and shapes of single moving edges (F). In the middle panel of D, ‡ indicates pairs of stimuli with different contrast polarity but same total luminance; # indicates those stimuli that had no match with stimuli of opposite contrast polarity.

light intensities between 251 and 6428 cd m^{-2} (SpectraScan PR655. Photo Research, Syracuse, NY, USA). Sample sizes were based on *a priori* power analysis performed in G*Power 3.1.9.2 (Faul et al., 2007, 2009) using effect sizes from pilot experiments. Contrast polarity was defined as the sign of the difference between the dots and the background [i.e. positive contrast for bright dots on a dark background (left in Fig. 1A) and negative contrast for dark dots on a bright background (right in Fig. 1A)].

Influence of visual scene properties on OKR performance

To test how scene properties such as contrast intensity and total luminance influence the OKR performance in scenes with positive and negative contrast, semi-intact preparations of *X. laevis* tadpoles were presented with sinusoidal large-field motion stimuli, in which contrast intensity and total luminance were systematically manipulated (Fig. 1D). Within each experiment, the order of stimuli was chosen randomly. Prior to the presentation of the first stimulus, a pattern of intermediate luminance was projected onto the screen. Between individual motion stimulus trials, the visual pattern of the preceding trial remained stationary on the screen.

Effect of contrast intensity

The effect of contrast intensity was tested in preparations (n=8) using sinusoidally moving random-dot scenes. Eight different visual scenes (contrast intensities between –100% for black dots on a white background and +100% for white dots on a dark background, four negative, four positive; see left panel in Fig. 1D) were presented in sparsely populated random-dot images (fill rate 13%).

Effect of total luminance

To explicitly test the effect of total luminance on OKR performance under both contrast polarity conditions, preparations (n=10) were presented with five different textures (fill rate 35%) with positive contrast and the same contrast magnitude but different total luminance levels (middle panel in Fig. 1D). In addition, five visual motion stimuli of different total luminance were presented with the same contrast magnitude but negative contrast. This resulted in a total of 10 stimuli. These stimuli were chosen such that eight stimuli formed four pairs (‡ in panel scheme in Fig. 1D): for each pair, the stimulus had a different contrast polarity but the overall same total luminance. The remaining two stimuli (# in middle panel in Fig. 1D)

had no match with opposite contrast polarity stimuli because of technical limitations of the display device.

Effect of contrast polarity

The third set of stimuli investigated the effect of contrast polarity on OKR amplitude. Preparations (n=12) were presented with two random-dot scenes, in which the total luminance was identical between both contrast polarities by filling 50% of the screen area with dots, while leaving the other 50% as background (right panel in Fig. 1D). Thereby, inverting contrast polarity did not change the ratio of bright versus dark patches on the screen and thus preserved the total luminance.

Influence of contour shapes

To test whether biases related to contrast polarity in the previous experimental conditions can be explained, at least partly, by a different structural organization of contours in positive as compared with negative contrast stimuli (concave versus convex edges), two additional stimulus protocols were presented to semi-intact *X. laevis* preparations (n=8). These stimuli were identical to the 50% fill rate stimuli in the previous condition, except that in the first of the two sets of experiments all dots were replaced by squares of the same area (Fig. 1E). This allowed identification of whether an influence of contrast polarity on the OKR is related to the shape of contours or rather to a foreground/background distinction.

To test whether the direction of the curvature of the contours (concave versus convex) influences OKR performance, the dots in the two maximal-contrast conditions (±100%; see left panel in Fig. 1D) were replaced by crescent-shaped contours with the same area and radius of the curvature (right panel in Fig. 1E). This resulted in four different visual stimuli, presented to the semi-intact preparations (n=6): positive and negative contrast with the opening either in or against the visual motion direction (to the left or to the right; see right panel in Fig. 1E). Because of the asymmetry of the contours, the stimuli were presented at constant velocity of 10 deg s^{-1} in the counter-clockwise direction.

Influence of contrast polarity-related biases of multi-unit optic nerve spike discharge

To elucidate whether contrast polarity related bias of the OKR is a property of retinal motion detection or an emerging feature during further signal processing in central visual relay centers, a subset of the previously described stimuli was presented to isolated *X. laevis* eyes while recording multi-unit spike activity from the severed optic nerve.

Optic nerve discharge in response to single moving edges

To evaluate the spike discharge pattern in the optic nerve, induced by a moving edge, a single vertical edge (height=2.5 mm, 1.8 deg visual angle) was moved through the isolated eye's field of view at a constant stimulus velocity of 10 deg s^{-1} in the temporo-nasal direction (Fig. 1F). The edge had one of three shapes (concave, CV; convex, CX; straight, ST), was shown either in front of a dark (positive/+) or bright (negative/−) background (Fig. 1F), and was a local change of light intensity either from dark to bright (ON) or from bright to dark (OFF).

Data analysis and statistics

The critical level of significance for all statistical comparisons was chosen as $\alpha<0.05$ unless otherwise stated. The influence of contrast intensity and contrast polarity was tested by a two-way repeated-measures ANOVA, with the factors contrast intensity and contrast polarity. The correlation between total texture luminance and normalized OKR amplitude was analyzed by performing a linear regression analysis, using the model:

$$A = \beta_1 + \beta_2 \times L, \quad (2)$$

individually for both contrast polarities with A as the relative OKR amplitude and L as the relative normalized total luminance; β_2 is the slope of the regression curve and indicates the sensitivity of the OKR amplitude to total luminance changes, and β_1 is the offset of the regression line.

Forty corresponding data points of the four pairs of overlapping luminance conditions (‡ in middle panel of Fig. 1D) were used to allow for unbiased comparison of positive and negative contrast stimuli. The slope of the regression was then compared between the responses to positive and negative contrast stimuli, using a bootstrap approach: in 100,000 permutations, 10 values were randomly drawn from the OKR amplitudes obtained from the four pairs of overlapping luminance conditions each, resulting in 40 data points in total. The model was then fitted as described above to each randomly drawn dataset to generate a distribution for the β_2 parameter, centered on its mean μ_2. Significance was then assessed by counting the relative amount of fits to random permutations, which had $|\beta_{2,perm}-\mu_2|>|\beta_{2,data}-\mu_2|$, and comparing with the critical value of significance. OKR amplitude differences between the two contrast polarities in the 50% fill rate textures were tested using a paired t-test.

RESULTS

Activation of horizontal optokinetic responses in *X. laevis* tadpoles

Large-field sinusoidal image motion of a black-and-white grating provokes phase-coupled following movements of both eyes in semi-intact *in vitro* preparations of *X. laevis* tadpoles (Schuller et al., 2014). This OKR represents the sensory feedback component of gaze stabilization during head/body motion (Collewijn, 1969; Straka and Dieringer, 2004). Pilot experiments in semi-intact *X. laevis* preparations using a sinusoidally oscillating large-field random-dot pattern in the present study evoked corresponding responses (Figs 1B, 2Ai,ii). Stimulus frequencies of 0.1–0.2 Hz and peak velocities of ±10 deg s^{-1} were able to elicit robust eye movements at mid-larval stages of this amphibian species (red trace in Fig. 2Ai,ii). The pilot experiments also revealed that the magnitudes of the evoked optokinetic responses depended not only on frequency and amplitude of the motion stimulus, but also on contrast polarity, i.e. bright dots on a dark background or vice versa (compare red and blue traces in Fig. 2Ai,ii,Bi,ii,Ci,ii). This result suggests that the contrast of a moving visual scene plays an important role for reflex performance. Thus, the first set of experiments systematically explored the influence of contrast polarity on the amplitude of the OKR.

Influence of visual stimulus parameters on OKR performance

The effect of contrast polarity on the OKR of *X. laevis* tadpoles was investigated by presenting four different contrast magnitudes of dots versus background (n=8 preparations). The random-dot stimuli had either a positive (dots were brighter than the background; see left scheme in Fig. 1A) or a negative contrast (dots were darker than the background; see right scheme in Fig. 1A). The systematic variation of this parameter revealed a gradual diminution of the OKR response amplitude with decreasing stimulus contrast, for both contrast polarities ($F_{3,52}$=24.17, P<0.001, η^2=0.30; see red and blue traces in Fig. 2Bi,ii,Ci,ii, respectively; Fig. 3A). This reduction in OKR performance with decreasing contrast magnitude was very

Journal of Experimental Biology (2017) 220, 4213-4224 doi:10.1242/jeb.167700

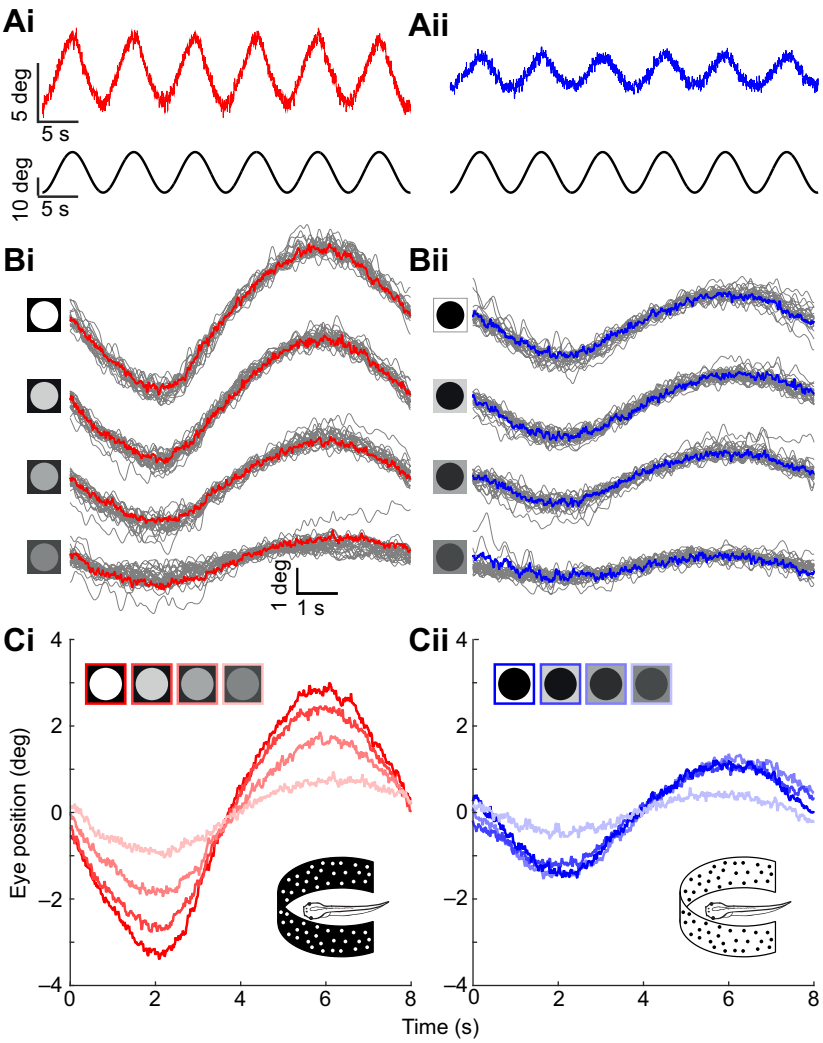

Fig. 2. Dependency of horizontal OKR amplitude on contrast polarity and intensity. (A) Representative examples of horizontal positional oscillations of the left eye (upper red and blue traces) extracted from video sequences during sinusoidal large-field image motion (frequency: 0.125 Hz, peak velocity: ±10 deg s^{-1}; lower traces) of a random-dot pattern with positive (red, Ai) and negative contrast (blue, Aii); calibration bars on the left also apply to the traces on the right. (B) Overlay of successive single cycles (gray lines) and averages (red and blue lines) for motion stimuli with different positive (Bi) and negative (Bii) contrast intensities as indicated by the icons to the left of the traces. (C) Averaged responses over a single cycle during visual motion stimulation with four textures of decreasing contrast intensity (indicated by color saturation) for positive (red, Ci) and negative (blue, Cii) contrast polarity; icons in the upper left corner depict the different contrast intensities.

similar between different preparations as indicated by the relatively small variability across different experiments (gray lines in Fig. 3A). In addition, a pronounced asymmetry was observed when varying contrast polarity (Fig. 3A). Response amplitudes were significantly larger for random-dot patterns with a positive compared with those with a negative contrast ($F_{1,52}$=57.62, P<0.001, η^2=0.24). In fact, at the same contrast intensity, the average OKR response to stimuli with a positive contrast out-sized the responses that were evoked by stimuli with a negative contrast by a factor of 2.24±1.01 (n=8). This indicates that the OKR performance depends on both contrast magnitude and contrast polarity.

The effect of contrast polarity on OKR performance under different total luminance conditions was tested in another group of semi-intact *X. laevis* tadpole preparations (n=10) by presenting motion stimuli with different textures (fill rate 35%). These stimuli had the same magnitude of contrast, but different total luminance levels and either positive or negative contrast polarity, resulting in a total of 10 different stimuli (see middle panel in Fig. 1D). To compare the effect of stimuli with opposite contrast polarity, the luminance for dots and background was chosen such that the total luminance was matched in four pairs of stimuli with positive and negative contrast (marked by ‡ in Fig. 3B). Even though the obtained results were somewhat variable between different preparations (see individual red and blue lines in Fig. 3B), OKR amplitudes nonetheless exhibited a clear and highly significant negative correlation with the total luminance of the visual scene (r_{99}=−0.691, P<0.001, d.f.=99). The two individual regression fits resulted in slopes of β_2=−2.65 for bright dots on a dark background and β_2=−1.44 for dark dots on a bright background. The two slope values were significantly different (positive contrast: P=0.021; negative contrast: P=0.022) compared with the mean slope of the bootstrap permutations. Accordingly, at lower overall brightness, the effect of contrast polarity is more pronounced, but vanishes for stimuli with higher total luminance (Fig. 3B). This indicates that contrast polarity differentially influences the OKR of *X. laevis* tadpoles depending on the total luminance of the optokinetic stimulus pattern.

Further, a potential impact of variations in contrast intensity and total image luminance was tested by presenting a moving scene in which 50% of the screen area was filled with dots, while the other half was a uniform background (n=12; right panel in Fig. 1D). Thereby, the presented stimuli with inverse contrast polarity differed only by having either a positive or a negative contrast, but neither in total luminance nor in contrast magnitude. This experimental approach confirmed the asymmetry of OKR response amplitudes for motion stimuli with different contrast polarities (Fig. 3C). Accordingly, the OKR amplitude was significantly larger (t_{11}=2.97, P=0.0126, d=0.64; Fig. 3C) with bright dots on dark background than with dark dots on bright background. Again, responses evoked by stimuli with positive contrast out-sized those

Journal of Experimental Biology (2017) 220, 4213-4224 doi:10.1242/jeb.167700

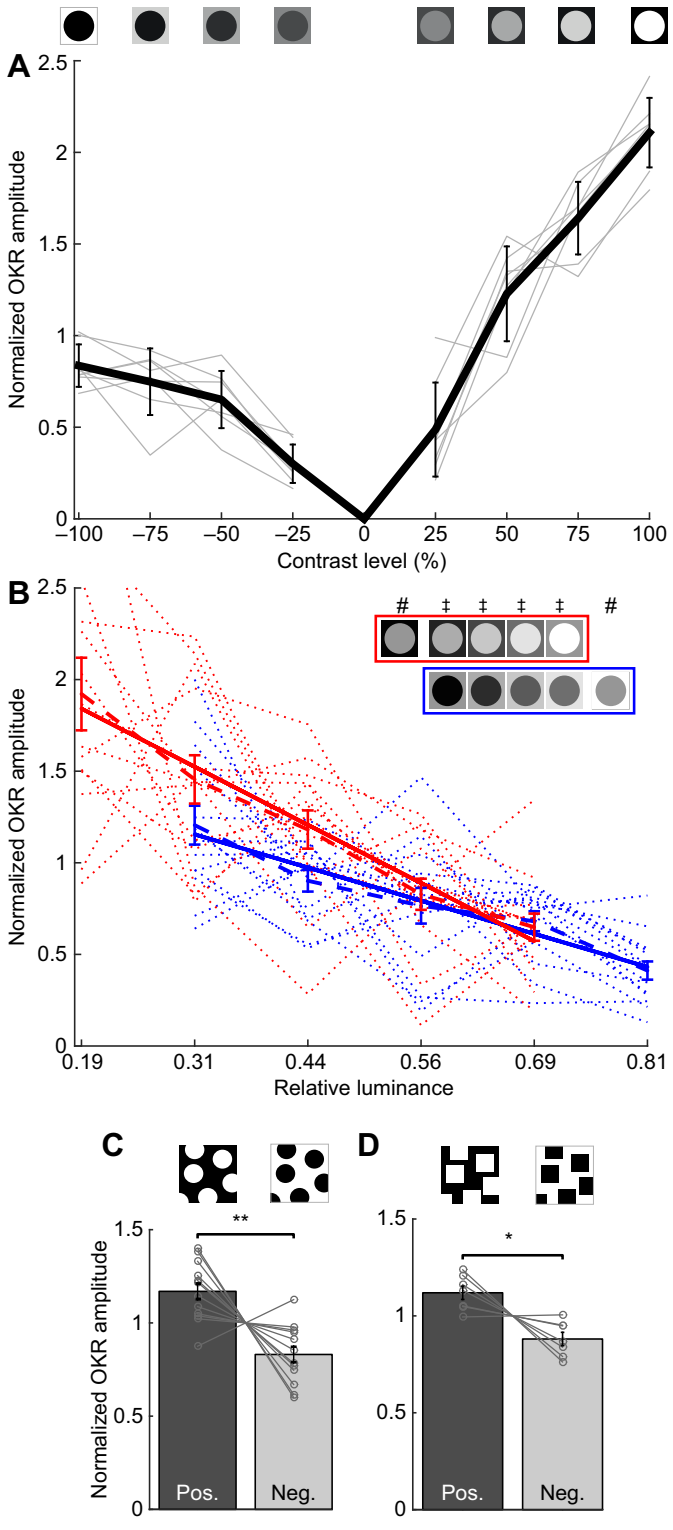

Fig. 3. Influence of large-field visual image properties on OKR performance. (A) Dependency of OKR amplitudes on contrast intensity of the random-dot pattern with positive (+) and negative contrast (–); note the asymmetry of responses to stimuli with opposite contrast polarity. Light gray lines represent data from individual experiments; the black line indicates the mean (±s.d.). (B) Dependency of the normalized OKR amplitude on relative luminance, normalized to the maximal brightness of the projectors (6428 cd m^{-2}). Dotted lines represent data from individual preparations, dashed lines indicate the mean (±s.d.) and solid lines the linear regression for positive (red; slope=–2.65, r^2=0.49) and negative contrast polarities (blue; slope=–1.44, r^2=0.45). In B, ‡ indicates pairs of stimuli with different contrast polarity but same total luminance; # indicates those stimuli that had no match with stimuli of opposite contrast polarity. (C,D) Bar plots depicting normalized OKR amplitudes under equiluminant conditions of stimulus patterns with circular (C) and square contours (D) and positive (dark gray) and negative contrast polarity (light gray). *P<0.05; **P<0.01. Icons above the plots in A–D depict the image properties of the different visual stimuli. Amplitudes in A–D were normalized to the mean amplitude for each preparation in the corresponding experimental conditions.

that were elicited with negative contrast stimuli by a factor of 1.49±0.49 (n=12). However, the smaller relative difference between the responses to the presented textures compared with the previous result (Fig. 3B) suggests that the effect of contrast polarity inversion was complemented in the previous experiments by concurrent changes in image brightness. This difference can be attributed to two structural variations in the image pattern that were caused by changing contrast polarity. One possibility is that the signal processing within the OKR circuitry is able to dissociate between foreground (dots) and background (one large connected area between the dots) and adjust its response based on this distinction. Alternatively, the OKR amplitude differs as a result of changing the curvature of contours from convex to concave and vice versa.

A potential impact of contour shape (convex versus concave curvature) on OKR performance was therefore tested by presenting a set of stimuli in which 50% of the area was filled with squares of either positive or negative contrast polarity (left panel in Figs 1E, 3D). Compatible with the dependency of the OKR magnitude on contrast polarity, the optokinetic response amplitude was significantly higher for stimuli with a positive compared with a negative contrast by a factor of 1.29±0.24 (t_6=3.48, P=0.013, d=2.63). This suggests that contour curvature is not the main cause for the observed differences related to contrast polarity.

This conclusion was further supported by another set of experiments that directly tested the impact of contour curvature on OKR performance. In these experiments, the presented images consisted of randomly scattered crescent-shaped contours (13% fill rate) with the opening either in or against the motion direction (Figs 1F, 4A). These direction-specific stimulus shapes with a positive or a negative contrast (left and right schemes in Fig. 4A) were presented at a constant velocity in one direction. In contrast to responses evoked by sinusoidal motion stimuli (e.g. Fig. 2Ai,ii), constant velocity visual motion elicited nystagmic eye movements that consisted of slow following movements in the stimulus motion direction interrupted by resetting fast phases in the opposite direction (Fig. 4B). This allowed quantifying two parameters of the OKR: slow-phase eye velocity, which was calculated as the average slope of the slow following movement (Fig. 4B) and the number of resetting fast phases over the stimulus period of 120 s.

Systematic variations of contrast polarity revealed consistent differences with respect to both parameters. Positive contrast stimuli (white crescent shapes on black background; red traces in Fig. 4C) evoked an OKR with a significantly higher slow-phase eye velocity and more fast phases independent of the orientation of the crescent-shaped pattern relative to the stimulus direction (compare red and blue traces in Fig. 4C). This is illustrated by the highly significant main effect of contrast polarity on the velocity of the slow following eye movements (compare red and blue bars in Fig. 4Di; repeated-measures ANOVA; $F_{1,19}$=138.4, η^2=0.71) and the number of fast phases (compare red and blue bars in Fig. 4Dii; repeated-measures ANOVA; $F_{1,19}$=26.01, η^2=0.44).

At variance with this result, the orientation of the crescent-shaped curvature with respect to the motion direction had no impact on

Journal of Experimental Biology (2017) 220, 4213-4224 doi:10.1242/jeb.167700

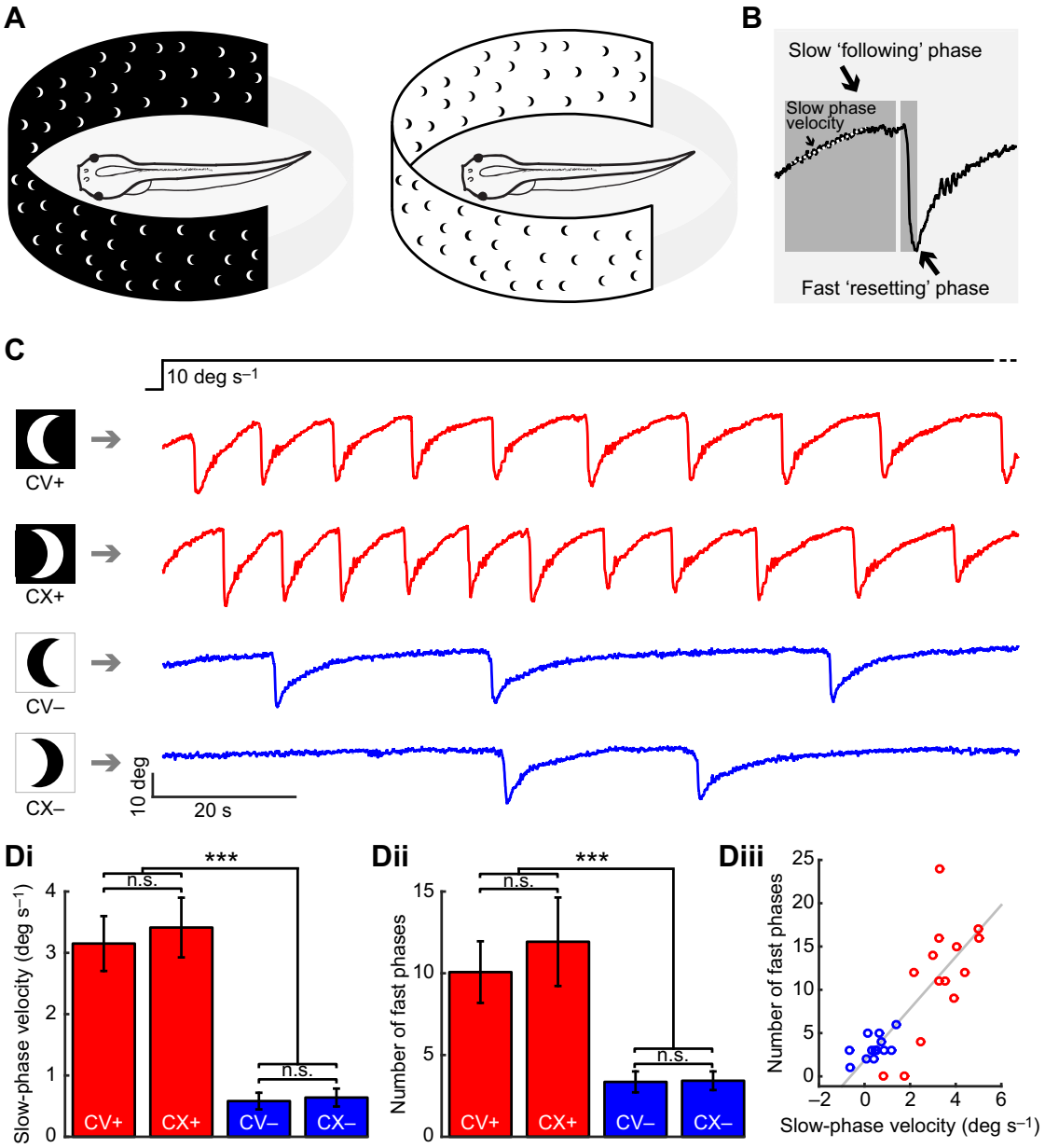

Fig. 4. Influence of contour shape on OKR performance. (A) Schematic illustrating the cylindrical large-field visual projection of crescent-shaped contours with positive (left) and negative (right) contrast polarity rotating at a constant velocity of 10 deg s^{-1}. (B) Typical nystagmic eye movement during unidirectional constant velocity image motion, consisting of slow following phases (white dotted line) interrupted by resetting fast phases. (C) Representative examples of nystagmic movements of the left eye during constant velocity image motion of crescent-shaped contours in temporo-nasal direction with positive (+, red traces) and negative (–, blue traces) contrast polarity and different orientations of the curvature [concave (CV) versus convex (CX)]. (D) Bar plots comparing average slow-phase velocity (Di) and number of fast phases (Dii) of eye movements evoked by constant velocity large-field image motion of crescent-shaped contours with positive (CV+, CX+, red) and negative contrast (CV–, CX–, blue); dependency of the number of fast phases on slow-phase eye velocity (Diii) for constant velocity crescent-shaped contour images with positive (red; n=14) and negative contrast (blue; n=14). ***P<0.001 in Di,ii (Wilcoxon signed-rank test; n=14); n.s., not significant.

OKR performance. Both, slow-phase velocity and number of fast phases were similar for the OKR elicited with concave and convex crescent shaped patterns (compare CV with CX traces in Fig. 4C) and applied for positive (red traces in Fig. 4C) as well as for negative contrast stimuli, respectively (blue traces in Fig. 4C). Thus, no significant main effect of the crescent curvature nor a significant interaction between curvature and contrast polarity was found for the slow-phase eye velocity (main effect: $F_{1,19}$=0.49, P=0.50, interaction: $F_{1,18}$=0.19, P=0.67) and number of fast phases (main effect: $F_{1,19}$=0.71, P=0.42, interaction: $F_{1,18}$=0.09, P=0.77; Fig. 4Di,ii). The tight link between slow-phase eye velocity and number of induced fast phases of the optokinetic response is further indicated by the close correlation between both parameters (r=0.82, n=28, P<0.001; Fig. 4Diii). This is likely due to the fact that the neuronal correlate responsible for generating higher slow-phase eye velocities during an OKR also causes fast-phase generating neuronal substrates to reach the activation threshold in a shorter time and thereby triggers fast phases more often. In contrast, the higher slow-phase eye velocity during visual motion stimulation with a positive contrast might derive from a

Journal of Experimental Biology (2017) 220, 4213-4224 doi:10.1242/jeb.167700

differential activation of motion detection circuits within the retina.

Optic nerve discharge activity during large-field visual motion stimulation

The implementation of a contrast polarity-biased motion detection system at the retinal level was tested by extracellular recordings of retinal ganglion cell activity as multi-unit spike discharge from the severed optic nerve in isolated *X. laevis* eye preparations (Fig. 5A). During sinusoidal horizontal large-field image motion, the multi-unit optic nerve discharge was cyclically modulated for both contrast polarities, i.e. white dots on a black background or black dots on a white background (Fig. 5B). However, motion stimuli with a positive contrast consistently yielded a more pronounced and robust discharge modulation (compare red and blue traces in Fig. 5B). Because the multi-unit recordings likely included units with a motion-sensitivity for either of the two stimulus directions, the population activity in the optic nerve could not be dissociated for naso-temporal or temporo-nasal motion. Accordingly, the multi-unit optic nerve firing rate was quantified by the bidirectional maximal discharge for further analysis. Despite the likely presence of different motion-sensitive retinal ganglion cells in the recordings with sensitivities to one or the other stimulus direction, the multi-unit discharge of the optic nerve proved to be a reliable estimate for the efficacy of large-field motion stimulus velocity.

The influence of contrast polarity and total luminance of the visual scene on retinal ganglion cell spike activity during large-field image motion was further tested with the same protocol described above for OKR performance (see left and middle panels in Fig. 1D). Accordingly, the effect of contrast polarity on modulated optic nerve discharge was evaluated by presenting four different contrast magnitudes of dots versus background (n=6 preparations, red and blue dotted lines in Fig. 5C). The differential influence of contrast polarity on the discharge modulation magnitude was more pronounced at low total luminance levels, and gradually decreased with higher light intensities (solid red and blue lines in Fig. 5C). This dependency is very similar to the impact of total luminance on the amplitude of the OKR (Fig. 3B; see dashed red and blue lines in Fig. 5C). In addition, the changes in modulation depth during the 50% fill rate stimulus conditions indicated that the modulation depth was significantly larger in response to positive than to negative contrast stimuli (dots: t_6=3.10, P=0.021, d=2.35; squares: t_6=2.95, P=0.026, d=2.23), compatible with the example shown in Fig. 5B. Moreover, the effect of contrast polarity was also very similar for dots and squares, suggesting that contour shape plays at most a minor role for retinal motion detection (left and right bar plot in Fig. 5D). These results indicate that the multi-

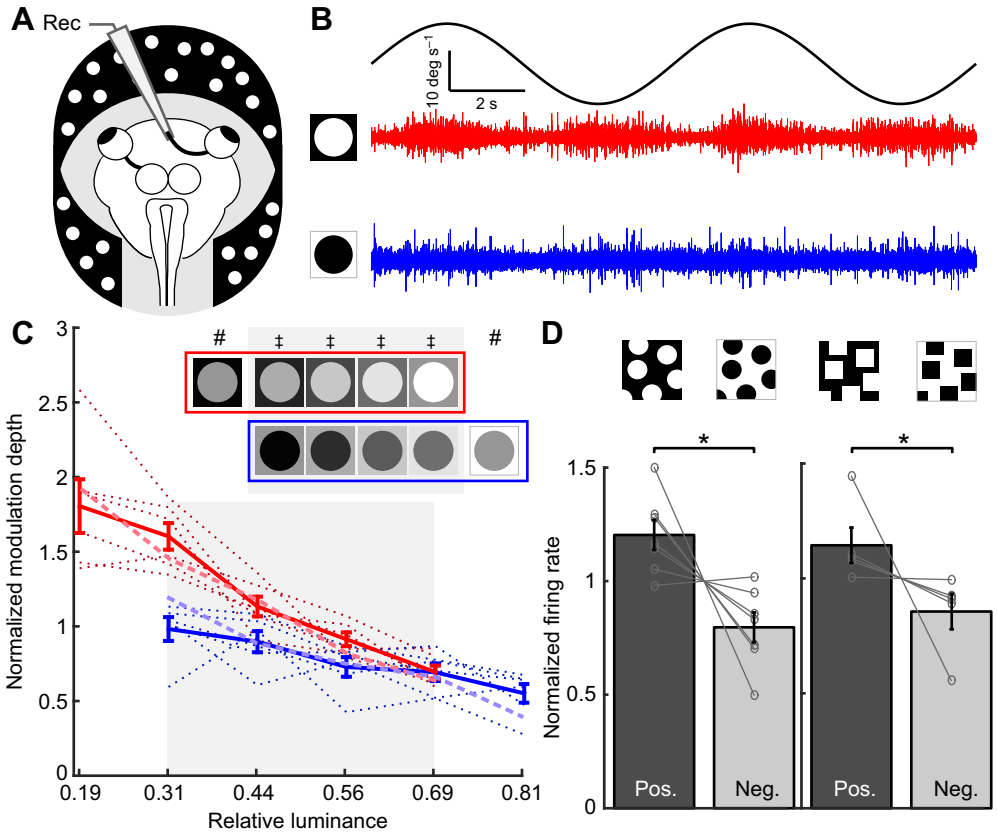

Fig. 5. Influence of large-field visual image properties on multi-unit optic nerve spike discharge. (A) Schematic illustrating the experimental setting for extracellular recordings of the severed right optic nerve with suction electrodes. (B) Representative example of modulated multi-unit optic nerve spike discharge during sinusoidal rotation (frequency: 0.125 Hz; peak velocity: ±10 deg s^{-1}) of a large-field visual scene with circular contours of positive (red) and negative (blue) contrast. (C) Dependency of the normalized discharge modulation depth on relative luminance. Dotted lines represent data from individual preparations for positive and negative contrast polarities and solid lines the mean (±s.d.); dashed red and blue lines indicate corresponding relative changes in OKR amplitude over the same range of relative luminance from Fig. 3B. In C, ‡ indicates pairs of stimuli with different contrast polarity but same total luminance; # indicates those stimuli that had no match with stimuli of opposite contrast polarity. (D) Bar plots depicting the normalized firing rate of multi-unit optic nerve discharge under equiluminant conditions of motion stimuli with circular (left) and square contours (right) and positive (dark gray) and negative (light gray) contrast polarity. *P<0.05. Icons above the plots in C,D depict the image properties of the different visual stimuli. Normalization in C,D was performed with respect to the mean firing rate for each preparation in the corresponding experimental conditions.

Journal of Experimental Biology

Journal of Experimental Biology (2017) 220, 4213-4224 doi:10.1242/jeb.167700

unit optic nerve discharge during large-field image motion exhibited a dependency on basic contrast and luminance parameters similar to that of the horizontal OKR behavior, and suggests that the differential signal processing of contrast and luminance within the retina is the origin of this effect.

Optic nerve responses to individual moving edges

All motion stimuli employed so far in the present study consisted of different moving shapes (dots, squares, crescent shapes) that were randomly scattered across the visual scene. The magnitude of the optic nerve discharge, however, might depend on the entirety of large-field image properties (i.e. explicit distinction between foreground and background) or on the characteristics of individual moving edges that move through the visual field in any of the used stimulus patterns. In fact, every moving shape consisted of two relevant moving vertical edges: the leading edge, facing the motion direction, and the trailing edge, at the rear end. Depending on the contrast polarity of the respective stimulus pattern, the two edges have different characteristics. For positive contrast stimuli, the leading edge presents a light intensity increment (ON edge), while the trailing edge presents a light decrement (OFF edge), and vice versa for negative contrast stimuli.

In order to elucidate the impact of moving edges, several sets of experiments were conducted that tested the influence of single edges moving through the visual field under different conditions on the magnitude of the multi-unit optic nerve discharge (Fig. 6A). In a first set of experiments, a single moving edge with a height of 2.5 mm (vertical visual angle 1.8 deg) was presented in front of a dark (+) or bright background (−) and with three different shapes (see upper row in Fig. 6B; concave, CV; convex, CX; straight, ST). Multi-unit neuronal optic nerve spike activity evoked by continuous motion of the edge (10 deg s^{-1}; 120 s) was independent of edge shape (repeated-measures ANOVA, $F_{2,89}$=0.05, P=0.95), but showed a highly significant difference related to the background ($F_{1,89}$=56.19,

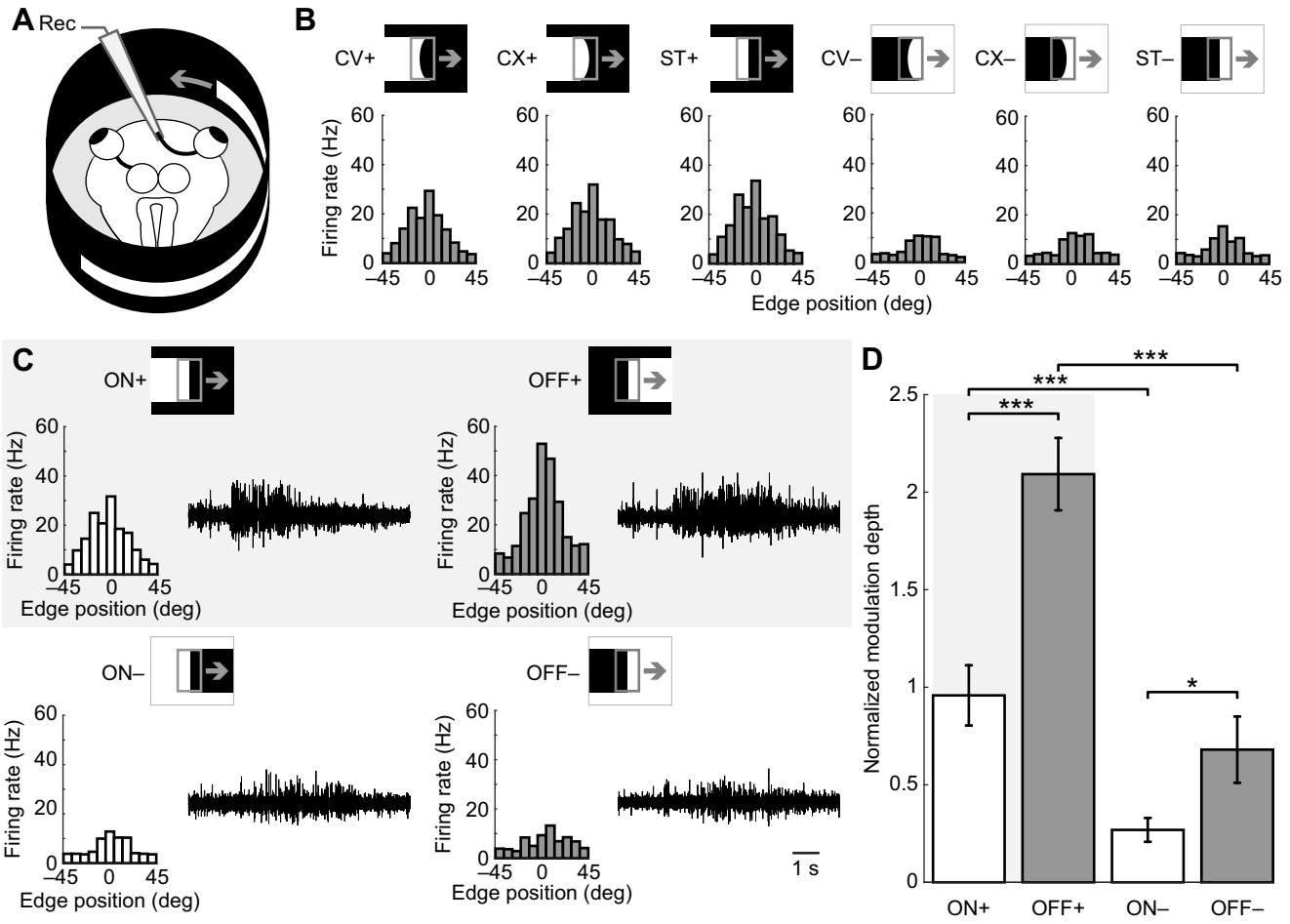

Fig. 6. Multi-unit optic nerve discharge in response to moving single edges. (A) Schematic illustrating the experimental setting for extracellular recordings of the severed right optic nerve with suction electrodes during motion of a long horizontal bar (180 deg) with either positive or negative contrast polarity at constant velocity in the temporo-nasal direction at 10 deg s^{-1} for stimulation of the eye with a single moving vertical edge. (B) Comparison of multi-unit optic nerve discharge rates over a range of 90 deg centered on the right eye during motion of a horizontal bar with different edge shapes (CV, concave; CX, convex; ST, straight) and positive (+) or negative (−) contrast polarity; gray arrows indicate the motion direction. (C) Multi-unit optic nerve discharge (traces in black) and firing rates over a range of 90 deg centered on the right eye (open and solid bar plots) during motion of a horizontal bar with a straight moving vertical ON or OFF edge in front of a dark (+) or bright (−) background (indicated by icons above spike discharge traces); note that ON (ON+, ON−) and OFF edges (OFF+, OFF−) were identical in their respective horizontal neighborhoods and only differed in the vertical surroundings. Calibration bar on the bottom right applies to all traces. (D) Bar plots depicting the average modulation depth (normalized to the mean modulation depth per preparation in all corresponding conditions) of multi-unit optic nerve discharge in response to moving bars with ON and OFF edges in front of a dark (ON+, OFF+) or bright background (ON−, OFF−). *P<0.05; ***P<0.001 (Wilcoxon signed-rank test; n=14).

Journal of Experimental Biology

$P<0.001$, $\eta^2=0.36$; Fig. 6B). This indicated that for a given contrast polarity, the curvature of an edge was not a discriminating factor for motion detection.

Because edge shape was not a confounding factor, we next assessed a potential impact of edge type (ON edge or OFF edge) and contrast polarity (dark or bright background) on the multi-unit optic nerve discharge using moving straight vertical edges (Fig. 6C). In agreement with the general definition, ON edges are characterized by a change in intensity of the horizontal moving bar from black to white, while OFF edges mark a change of the bar from white to black. Accordingly, stimuli were constructed such that bars with the same edge type (ON+/ON− or OFF+/OFF−) were identical in the horizontal neighborhood of the moving edge (i.e. dark in front of the ON edge, bright behind the ON edge, and vice versa for OFF edges; see Fig. 6C). Accordingly, these stimuli only differed in the vertical neighborhood under the two contrast polarity conditions (dark background for positive contrast and bright background for negative contrast). Recordings of multi-unit optic nerve discharge during image motion revealed considerable differences in the firing rate magnitude during the four different stimulus conditions (spike discharge in Fig. 6C). In fact, OFF edges evoked on average significantly higher motion-related optic nerve discharge rates (repeated-measures ANOVA, $F_{1,89}=51.2$, $P<0.001$, $\eta^2=0.19$; compare white and gray bars in Fig. 6D). However, this difference was much less pronounced for negative compared with positive contrast edges (compare bottom with top traces in Fig. 6C and right and left bars in Fig. 6D). In fact, responses to light decrements (OFF edges) were on average more than twice as strong as responses to light increments. This suggests that motion detection in the retina of larval *X. laevis* is predominantly performed by the OFF pathway. Moreover, the contrast polarity-related bias observed for dots and for squares was also reproduced at the level of single moving edges. This was demonstrated by a significant main effect of contrast polarity ($F_{1,89}=94.84$, $P<0.001$, $\eta^2=0.36$) as well as a significant interaction between edge type and contrast polarity ($F_{1,89}=10.2$, $P=0.002$, $\eta^2=0.04$), suggesting that the stimulus velocity-related retinal ganglion cell discharge is influenced by the light intensity in the vertical neighborhood of the horizontally moving edge.

DISCUSSION

OKR performance in *X. laevis* tadpoles is better for positive (bright dots on a dark background) than for negative contrast large-field visual stimuli. This effect is independent of contrast intensity, contour shape and motion pattern. Recordings of multi-unit optic nerve discharge during visual motion stimulation yielded similar results, thus indicating that the neuronal basis for this effect might originate from signal processing properties of the retinal circuitry.

OKR performance in semi-intact preparations

Gaze stabilization of retinal images during passive motion or self-motion requires an estimate of the velocity of the large-field visual world motion (Collewijn, 1969). This image velocity directly determines the performance of the OKR with the purpose of minimizing visual slip signals, thereby ensuring high acuity (Cohen et al., 1977). The horizontal OKR in amphibians is mediated by a short-latency reflex arc that involves retinal ganglion cells, a set of accessory optic neurons in the pretectum, and extraocular motoneurons that activate synergistic pairs of horizontal extraocular muscles of the two eyes (Cochran et al., 1984). Semi-intact preparations of *X. laevis* tadpoles are ideally suited to evoke and quantify this sensory-driven motor behavior (Straka and Simmers, 2012). Based on the presence of intact sensory elements (eyes), motor structures (eye muscles) and central nervous circuits as well as the experimental accessibility, this preparation facilitates studying the dynamic range of visual motion processing and the dependency of the behavioral performance on visual scene features.

The generally robust performance of the OKR in semi-intact *X. laevis* tadpole preparations at mid-larval stages in the present study is similar to that of a previous pilot study in these animals (Schuller et al., 2014) and also complies with expectations from *in vivo* experiments on adult frogs (Dieringer and Precht, 1982). Thus, the present *in vitro* approach represents a convenient method with high validity and accountability to decipher the influence of general visual scene properties on the performance of this visuo-motor behavior. The anatomically very similar layout of eyes and subcortical visual circuits in all anamniotes and a number of amniote vertebrates (Maximino, 2008; Masseck and Hoffmann, 2009a,b) make the visual system of *X. laevis* well suited to provide further insight into the basic mechanisms of image motion processing.

OKR performance is influenced by contrast polarity

Experimental manipulations of visual scene parameters in the current experiments indicated that OKR amplitudes varied strongly as a result of inverting contrast polarity of the visual scene. This dependency is remarkable, given that the stimulus texture with respect to number and intensity of contours is identical. Thus, the influence of contrast polarity differs from prior expectation based on, for example, spatiotemporal motion energy (Adelson and Bergen, 1985; Reichardt, 1987). According to this type of model, motion perception including visual stimulus velocity estimation should be unaffected by pure inversion of contrast polarity. However, this is not the case, even though this effect is most prominent at lower overall light levels. A uniform increase of the total luminance of the visual scene by a constant value caused a decrease in both the amplitude of the optokinetic response as well as in the influence of contrast polarity on OKR performance (Fig. 3B, red and blue lines). Interestingly, the slopes, intercept and point at which the contrast polarity effect vanished (intersection of the two lines) were very similar between the visuo-motor behavior and the spike discharge of the optic nerve. The generally corresponding effects of these visual scene parameters on the OKR and optic nerve discharge suggest that the origin of the dependency of OKR performance on large-field visual scene properties is due to a direct influence of these properties on retinal signal processing (see below). Accordingly, pretectal and extraocular motor processing of visual motion signals have at maximum a limited impact on the motion velocity estimate.

The asymmetry in OKR performance that is related to contrast polarity and likely caused by retinal velocity computations is not only expressed in the magnitude of the slow-phase eye velocity but also by the number of evoked fast phases during constant velocity stimulation (Fig. 4C,Dii). In general, fast-phase generation is directly related to the internal estimate of the visual surround velocity (Anastasio, 1996), and thus is influenced by those parameters that affect the estimation of the visual image slip velocity at retinal/central nervous system levels. The strong correlation between fast-phase number and slow-phase eye velocity supports this assumption. Accordingly, motor commands for slow-phase following eye movements as well as the neural signals for fast phases derive directly or indirectly from the same velocity estimate.

Functional relevance of OKR asymmetry

From a functional point of view, the OKR asymmetry appears counterintuitive at first. Most animals, including *X. laevis* tadpoles,

Journal of Experimental Biology

Journal of Experimental Biology (2017) 220, 4213-4224 doi:10.1242/jeb.167700

must cope with a large range of visual scenarios. This requires a robust estimate of the motion velocity of the visual scene to generate appropriate eye movements for a constant maintenance of high visual acuity. Thus, in complex environments enriched with stationary and moving objects, distinctions based on contrast polarity would facilitate the adjustment of visuo-motor responses to relevant portions of the possibly incoherent large-field visual motion. The preferential responsiveness to small bright objects in front of a dark background as shown in *X. laevis* tadpoles might be considered as a low-level functional interpretation of image motion. Comparable contrast polarity-related differences as reported here for the OKR performance of *X. laevis* tadpoles were described for zebrafish larvae, where large dark moving spots on a bright background elicit avoidance, while closed contours with negative contrast are interpreted as prey (Bianco and Engert, 2015). However, in contrast to the pretectal OKR pathway, the latter avoidance and approach behaviors are mediated by specific tectal pathways (Semmelhack et al., 2014). Because similar prey/non-prey distinctions were also found in adult frogs (Lettvin et al., 1959; Barlow and Hill, 1963), contrast-dependent motion estimation at early visual processing levels might be a general feature and the origin of differences in the performance of several reflexive or voluntary behaviors.

Optic nerve population activity encodes stimulus velocity

The population activity of the optic nerve is modulated with the velocity of a moving large-field visual scene. However, the strength of modulation depends on contrast polarity. This suggests that the information about image velocity is already encoded as population rate code at the level of the retinal ganglion cell axons in the optic nerve. The striking similarity between visual scene-related biases of ocular motor behavior and those of optic nerve discharge observed in this study (Figs 3, 5) suggests that ganglion cell population activity is interpreted as a velocity correlate by the OKR circuitry and directly forms the basis for the performance of this visuo-motor behavior, but without providing information about the specific direction of the motion. The information for both motion directions, i.e. temporo-nasal and naso-temporal, is likely processed in separate channels, which begin with motion-sensitive retinal ganglion cells and project as separate signaling pathways to different premotor nuclei in the pretectum (Fite et al., 1989; Masseck and Hoffmann, 2009b).

Retinal motion velocity signals in retinal circuits are influenced by contrast polarity

Directionally sensitive signals in neurons of the peripheral visual circuitry have been reported in numerous vertebrate (Barlow and Hill, 1963; Oyster et al., 1993; Pinsky et al., 2015) and invertebrate species (Haag et al., 2016) and appear to be a common feature in the processing of visual motion. The neuronal substrate is known to be organized in different information streams, which operate as edge detectors and respond to light increments (ON), decrements (OFF) or both (ON/OFF; Borst and Euler, 2011). In the vertebrate retina, these cells extract motion information but also perform an advanced processing of the incident image (Lettvin et al., 1959; Clifford and Ibbotson, 2002; Gollisch and Meister, 2010). In particular, neuronal computations in retinal ganglion cells allows, for example, toads to perceptually discriminate between prey and non-prey objects simply based on the sign of contrast (Ewert and Siefert, 1974). This notion is supported by pattern analyses based on image contrast in tectal and thalamic areas in these animals (Ewert and von Wietersheim, 1974). The organization of the visual scene, however, strongly influences the extraction of motion information. Even when presented with an identical velocity profile, retinal ganglion cell population activity in *X. laevis* is differently modulated depending on whether the image is presented with positive or negative contrast. One possible mechanism is based on different temporal characteristics in the interaction between ON and OFF edge detectors. Another cause of the contrast polarity-related asymmetry could be the change in curvature of ON and OFF edges: for positive contrast, a moving closed contour consists of a convex leading ON and a concave trailing OFF edge and vice versa for stimuli with negative contrast.

However, differential modulation of responses to ON or OFF edges depending on contour curvature was not observed in the present study, excluding this possibility as a relevant mechanism for the observed contrast polarity-dependent effects. Instead, our study suggests another mechanism that depends on the light intensity in the vertical neighborhood of horizontally moving edges (Fig. 6). Optic nerve population responses to a single moving vertical edge showed different activation patterns depending on whether the moving edge was presented on a bright or a dark background. This could be due to the receptive field size of retinal ganglion cells extending across the dimensions of the edge into the background area. High uniform light intensities illuminating the receptive field appear to suppress or inhibit responses of these neurons to moving contours, compatible with the weaker optic nerve discharge modulation during motion of random particles on a bright background. This is also consistent with our observation that the overall modulation depth as well as the difference related to inversion of contrast polarity decreases with higher overall luminance (Fig. 5C, red and blue lines). Accordingly, at strong light intensities, the background brightness appears to be intense enough to attenuate retinal ganglion cell discharge even for objects with a positive contrast (i.e. brighter than the background). In zebrafish, the OKR appears to be activated by the retinal ON but not the OFF pathway (Emran et al., 2007). Whether this is also the case for *X. laevis* remains unknown. However, because the relative decrease of retinal ganglion cell discharge modulation by a bright background was similar for responses to ON and to OFF edges (Fig. 6D), a direct correlate of retinal biases can be observed in the OKR, independent of which channel(s) drive the OKR.

Conclusions

Visuo-motor behavior and motion stimulus-related retinal output signal amplitudes are highly influenced by contrast polarity in otherwise identical visual scenes. This is likely due to retinal signal processing of moving edges that depends on the local context of the stimulus environment. For vertical edges moving in the horizontal plane, the light intensity in the area above and below the edges has a dominating impact on the computations underlying retinal motion processing. This directly translates into OKR performance, which scales in magnitude with the population discharge activity of retinal ganglion cells.

Acknowledgements

The authors thank the mechanical workshop of the Biocenter Martinsried for their help in assembling the experimental setup.

Competing interests

The authors declare no competing or financial interests.

Author contributions

Conceptualization: C.M.G., A.G.K.; Methodology: C.M.G., A.G.K.; Software: A.G.K.; Validation: C.M.G.; Formal analysis: C.M.G., A.G.K.; Investigation: C.M.G., A.G.K.; Writing - original draft: C.M.G., A.G.K.; Writing - review & editing: S.G., H.S.; Visualization: C.M.G., A.G.K.; Supervision: S.G., H.S.; Project administration: S.G., H.S.; Funding acquisition: S.G., H.S.

Funding
The authors acknowledge financial support from the German Science Foundation (Deutsche Forschungsgemeinschaft) (CRC 870; STR 478/3-1, GL 342/2-1 and RTG 2175), the German Federal Ministry of Education and Research (Bundesministerium für Bildung und Forschung; grant code 01 EO 0901) and the Bernstein Center for Computational Neuroscience Munich (BT-1).

References

Adelson, E. H. and Bergen, J. R. (1985). Spatiotemporal energy models for the perception of motion. *J. Optic. Soc. Am. A Opt. Image Sci.* **2**, 284-299.
Anastasio, T. J. (1996). A random walk model of fast-phase timing during optokinetic nystagmus. *Biol. Cybern.* **75**, 1-9.
Barlow, H. B. and Hill, R. M. (1963). Selective sensitivity to direction of movement in ganglion cells of the rabbit retina. *Science* **139**, 412-414.
Beck, J. C., Gilland, E., Baker, R. and Tank, D. W. (2004). Instrumentation for measuring oculomotor performance and plasticity in larval organisms. *Meth. Cell Biol.* **76**, 385-413.
Bianco, I. H. and Engert, F. (2015). Visuomotor transformations underlying hunting behavior in zebrafish. *Curr. Biol.* **25**, 831-846.
Borst, A. and Euler, T. (2011). Seeing things in motion: models, circuits, and mechanisms. *Neuron* **71**, 974-994.
Clifford, C. W. G. and Ibbotson, M. R. (2002). Fundamental mechanisms of visual motion detection: models, cells and functions. *Progr. Neurobiol.* **68**, 409-437.
Cochran, S. L., Dieringer, N. and Precht, W. (1984). Basic optokinetic-ocular reflex pathways in the frog. *J. Neurosci.* **4**, 43-57.
Cohen, B., Matsuo, V. and Raphan, T. (1977). Quantitative analysis of the velocity characteristics of optokinetic nystagmus and optokinetic after-nystagmus. *J. Physiol.* **270**, 321-344.
Collewijn, H. (1969). Optokinetic eye movements in the rabbit: input–output relations. *Vision Res.* **9**, 117-132.
Dieringer, N. and Precht, W. (1982). Compensatory head and eye movements in the frog and their contribution to stabilization of gaze. *Exp. Brain Res.* **47**, 394-406.
Donaghy, M. (1980). The contrast sensitivity, spatial resolution and velocity tuning of the cat's optokinetic reflex. *J. Physiol.* **300**, 353-365.
Emran, F., Rihel, J., Adolph, A. R., Wong, K. Y., Kraves, S. and Dowling, J. E. (2007). OFF ganglion cells cannot drive the optokinetic reflex in zebrafish. *Proc. Nat. Acad. Sci. USA* **104**, 19126-19131.
Enroth-Cugell, C. and Robson, J. G. (1966). The contrast sensitivity of retinal ganglion cells of the cat. *J. Physiol.* **187**, 517-552.
Ewert, J.-P. and Siefert, G. (1974). Neuronal correlates of seasonal changes in contrast-detection of prey catching behaviour in toads (*Bufo bufo L.*). *Vision Res.* **14**, 431-432.
Ewert, J.-P. and von Wietersheim, A. (1974). Musterauswertung durch Tectum- und Thalamus/Praetectum-Neurone im visuellen System der Kröte *Bufo bufo* (L.). *J. Comp. Physiol. A* **92**, 131-148.
Faul, F., Erdfelder, E., Lang, A.-G. and Buchner, A. (2007). G*Power 3: a flexible statistical power analysis program for the social, behavioral, and biomedical sciences. *Behav. Res. Meth.* **39**, 175-191.
Faul, F., Erdfelder, E., Buchner, A. and Lang, A.-G. (2009). Statistical power analyses using G*Power 3.1: tests for correlation and regression analyses. *Behav. Res. Meth.* **41**, 1149-1160.
Fite, K. V., Kwei-Levy, C. and Bengston, L. (1989). Neurophysiological investigation of the pretectal nucleus lentiformis mesencephali in *Rana pipiens*. *Brain, Behav. Evol.* **34**, 164-170.
Gollisch, T. and Meister, M. (2010). Eye smarter than scientists believed: neural computations in circuits of the retina. *Neuron* **65**, 150-164.
Haag, J., Arenz, A., Serbe, E., Gabbiani, F. and Borst, A. (2016). Complementary mechanisms create direction selectivity in the fly. *eLife* **5**, 175-181.
Hänzi, S. and Straka, H. (2016). *Schemes of Xenopus laevis tadpoles*. Figshare. doi:10.6084/m9.figshare.3841173.v2
Lambert, F. M., Combes, D., Simmers, J. and Straka, H. (2012). Gaze stabilization by efference copy signaling without sensory feedback during vertebrate locomotion. *Curr. Biol.* **22**, 1649-1658.
Lettvin, J. Y., Maturana, H. R., Maturana, H. R., Mcculloch, W. S. and Pitts, W. H. (1959). What the frog's eye tells the frog's brain. *Proc. IRE* **47**, 1940-1951.
Masseck, O. A. and Hoffmann, K.-P. (2009a). Comparative neurobiology of the optokinetic reflex. *Ann. N. Y. Acad. Sci.* **1164**, 430-439.
Masseck, O. A. and Hoffmann, K.-P. (2009b). Question of reference frames: visual direction-selective neurons in the accessory optic system of goldfish. *J. Neurophysiol.* **102**, 2781-2789.
Maximino, C. (2008). Evolutionary changes in the complexity of the tectum of nontetrapods: a cladistic approach. *PLoS ONE* **3**, e3582.
Nieuwkoop, P. D. and Faber, J. (1994). *Normal Table of Xenopus laevis (Daudin): a Systematical and Chronological Survey of the Development from the Fertilized Egg Till the End of Metamorphosis*. New York, USA: Garland.
Oyster, C. W., Amthor, F. R. and Takahashi, E. S. (1993). Dendritic architecture of ON-OFF direction-selective ganglion cells in the rabbit retina. *Vision Res.* **33**, 579-608.
Packer, O., Diller, L. C., Verweij, J., Lee, B. B., Pokorny, J., Williams, D. R., Dacey, D. M. and Brainard, D. H. (2001). Characterization and use of a digital light projector for vision research. *Vision Res.* **41**, 427-439.
Pinsky, E., Donchin, O. and Segev, R. (2015). Pharmacological study of direction selectivity in the archer fish retina. *J. Integr. Neurosci.* **14**, 473-490.
Ramlochansingh, C., Branoner, F., Chagnaud, B. P. and Straka, H. (2014). Efficacy of tricaine methanesulfonate (MS-222) as an anesthetic agent for blocking sensory-motor responses in *Xenopus laevis* tadpoles. *PLoS ONE,* **9**, e101606.
Reichardt, W. (1987). Evaluation of optical motion information by movement detectors. *J. Comp. Physiol. A* **161**, 533-547.
Schuller, J. M., Knorr, A. G., Glasauer, S. and Straka, H. (2014). Task-specific activation of extraocular motoneurons in *Xenopus laevis*. *Soc. Neurosci. Abstr.* **40**, 247.
Semmelhack, J. L., Donovan, J. C., Thiele, T. R., Kuehn, E., Laurell, E. and Baier, H. (2014). A dedicated visual pathway for prey detection in larval zebrafish. *Elife* **3**, E2391-E2398.
Straka, H. and Dieringer, N. (2004). Basic organization principles of the VOR: lessons from frogs. *Progr. Neurobiol.* **73**, 259-309.
Straka, H. and Simmers, J. (2012). *Xenopus laevis*: an ideal experimental model for studying the developmental dynamics of neural network assembly and sensory-motor computations. *Dev. Neurobiol.* **72**, 649-663.
von Uckermann, G., Lambert, F. M., Combes, D., Straka, H. and Simmers, J. (2016). Adaptive plasticity of spino-extraocular motor coupling during locomotion in metamorphosing *Xenopus laevis*. *J. Exp. Biol.* **219**, 1110-1121.